Current Biology 21, 1391–1396, August 23, 2011 ©2011 Elsevier Ltd All rights reserved DOI 10.1016/j.cub.2011.07.015

Report

Expansion-Repression Mechanism for Scaling the Dpp Activation Gradient in *Drosophila* Wing Imaginal Discs

Danny Ben-Zvi,[1] George Pyrowolakis,[2,3] Naama Barkai,[1,4,*] and Ben-Zion Shilo[1,*]
[1]Department of Molecular Genetics, Weizmann Institute of Science, Rehovot 76100, Israel
[2]Institute for Biology I, Albert-Ludwigs-University of Freiburg Hauptstrasse. 1, D-79104 Freiburg, Germany
[3]Centre for Biological Signaling Studies (BIOSS), Albert-Ludwigs-University of Freiburg Albertstrasse. 19, D-79104 Freiburg, Germany
[4]Department of Physics of Complex Systems, Weizmann Institute of Science, Rehovot 76100, Israel

Summary

Maintaining a proportionate body plan requires the adjustment or scaling of organ pattern with organ size. Scaling is a general property of developmental systems, yet little is known about its underlying molecular mechanisms. Using theoretical modeling, we examine how the Dpp activation gradient in the *Drosophila* wing imaginal disc scales with disc size. We predict that scaling is achieved through an expansion-repression mechanism [1] whose mediator is the widely diffusible protein Pentagone (Pent). Central to this mechanism is the repression of *pent* expression by Dpp signaling, which provides an effective size measurement, and the Pent-dependent expansion of the Dpp gradient, which adjusts the gradient with tissue size. We validate this mechanism experimentally by demonstrating that scaling requires Pent and further, that scaling is abolished when *pent* is ubiquitously expressed. The expansion-repression circuit can be readily implemented by a variety of molecular interactions, suggesting its general utilization for scaling morphogen gradients during development.

Introduction

The size of the developing organism is highly variable, depending on external nutrient conditions or genetic polymorphisms. Scaling of tissue pattern with tissue size is therefore required for ensuring a body plan of reproducible proportions. Scaling was demonstrated in a large number of systems [1–9] and was studied most extensively in the context of the *Drosophila* wing imaginal disc [10–12]. Two long-range gradients of the Wg and Dpp morphogens pattern the disc along the orthogonal dorsoventral (DV) and anterior-posterior (AP) axes, respectively. The scaling of the Dpp gradient with disc size was first demonstrated in mutants of the insulin pathway. In these mutants, disc size is significantly modulated, but the pattern remains unaffected, with scaling observed at the levels of the Dpp gradient itself, its activity pattern, and target-gene expression [10]. Notably, Dpp functions not only as a morphogen but also as a growth factor, facilitating disc growth [13–16], yet its gradient stabilizes rapidly relative to disc growth rate, suggesting that it is close to steady state during growth [10, 11]. It was recently shown that the Dpp gradient scales with disc size also during growth, such that the length scale of the Dpp gradient remains proportional to the size of the disc over at least a 2-fold increase in size [11].

Scaling of morphogen-induced pattern with tissue size requires the ability to measure tissue size and adjust the morphogen distribution accordingly. Most models of morphogen gradients do not account for scaling. Recently, we have shown that scaling is a natural property of a simple circuit motif, which we termed "expansion-repression" (Figure 1A) [1]. This motif is composed of two diffusible molecules, a morphogen and an expander, which are tightly interconnected: the morphogen represses expander production, limiting its secretion only to the distal part of the morphogenic field, whereas the expander (which is diffusible and stable) increases morphogen spreading in the entire field by facilitating its diffusion or inhibiting its degradation. The expander, in effect, measures the system size: it continues to accumulate, and consequently, the gradient continues to expand, until the morphogen levels are sufficiently high to repress expander expression even at the edge of the field (Figure 1B). Scaling of the full gradient with system size follows naturally, because the level of morphogen at the distal-most region is effectively pinned to the value required to repress expander expression.

The expansion-repression mechanism can be implemented by a variety of molecular mechanisms and is relatively independent of the precise biochemical parameters. We examined whether this motif is found also within the Dpp patterning network. Dpp signals by binding to its receptor Thickveins (Tkv), modulating the expression of downstream genes, some of which function in a feedback circuit shaping the Dpp gradient itself [17]. For example, Dpp attenuates *tkv* expression, whereas Tkv modulates both Dpp signaling and its degradation by endocytosis [10, 18–20]. Similarly, Dpp also reduces the expression of *dally*, a heparan sulfate proteoglycan, which affects the mobility and stability of Dpp [21–25]. Neither Dally nor Tkv, however, can function as expanders, because they do not diffuse and therefore modulate the gradient mostly locally. Moreover, they are both expressed at significant levels also close to the source of Dpp. We noticed that a newly identified component of the circuit, Pentagone (Pent), does realize an expansion-repression motif [26]. *pent* is repressed by Dpp signaling, and it expands the Dpp gradient through interaction with Dally. Crucially, it is widely diffusible and stable, enabling propagation of information from the edges of the disc toward the source of the gradient (Figures 1C and 1D).

Results and Discussion

Numerical modeling of the interactions between Dpp, Tkv, Dally, and Pent confirmed that this simplified Dpp-patterning network can implement the expansion-repression mechanism, leading to scaling of the Dpp activity gradient with the size of the disc over a broad range of parameters (Figures 1F–1H; see also Figure S1 available online). In the particular implementation shown, we assumed that the interaction of Pent with Dally reduces the affinity between Tkv and Dpp,

*Correspondence: naama.barkai@weizmann.ac.il (N.B.), benny.shilo@weizmann.ac.il (B.-Z.S.)

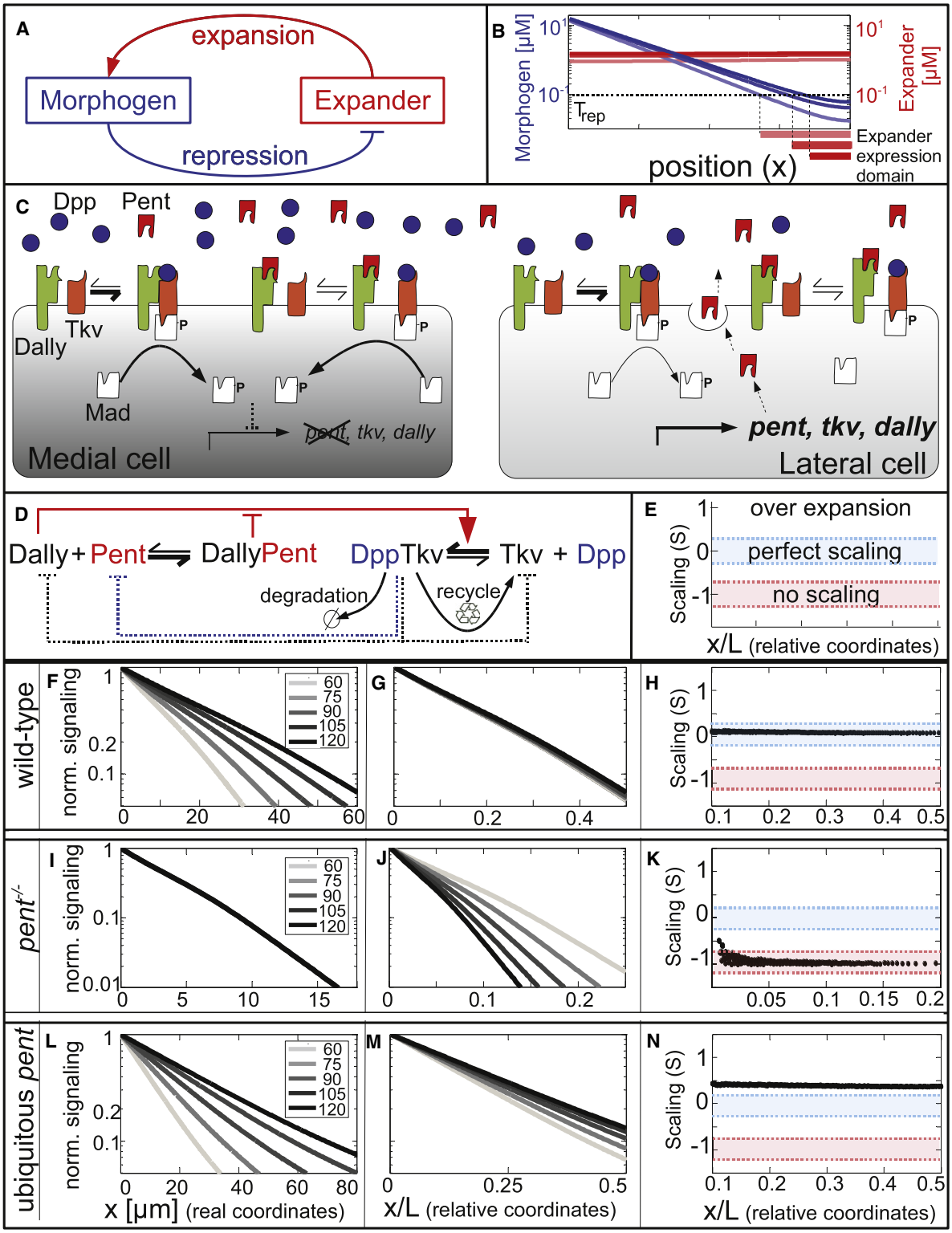

Figure 1. The Expansion-Repression Feedback Mechanism in the Wing Imaginal Disc

(A) The expansion-repression feedback motif: morphogen (blue) represses the expression of an expander (red). The expander, which is diffusible and stable, expands the morphogen gradient by increasing the morphogen diffusion and/or reducing its degradation rate.

(B) Dynamics of the expansion-repression mechanism: light shades of blue and red stand for early stages in the dynamics; darker shades of blue and red represent later stages. Morphogen signaling (blue) represses the expression of the expander (red) above the threshold T_{rep}. The expander expression domain is shown below the x axis in red bars. Accumulation of the expander leads to the expansion of morphogen gradient, which causes the reduction in the expression domain of the expander, until the expander is repressed in virtually the entire field, whereas morphogen levels at the edge of the field are close to T_{rep}. See Supplemental Information for model equations and Table S1 for parameters.

thereby lowering Dpp degradation via endocytosis, in accordance with recent studies [11]. In this case, the decrease in Dpp degradation rate during growth of the disc can be attributed to Pent activity as an expander. Notably, the expansion-repression mechanism is relatively insensitive to the molecular details of the putative implementation. Other realizations of Dally-Pent interaction, in which Pent effectively increases Dpp diffusion, provide equally robust scaling as long as the Dpp-Pent expansion-repression motif is maintained (Figure S1).

To analyze the simulation results quantitatively and define their robustness, we introduced a scaling measure, S, which quantifies the accuracy of scaling at each position, independent of the shape of the gradient (Experimental Procedures). Briefly, S describes the difference between signaling profiles measured in the relative coordinate x/L in discs of different sizes, at each position along the AP axis. S is normalized such that S = 0 when scaling is perfect, and S = −1 when there is no scaling at all. Intermediate values (−1 < S < 0) indicate partial scaling, namely, insufficient expansion of the gradient compared to its growth, whereas positive values of S describe an expansion overshoot, where the gradient expands more than it should have relative to the size of the disc (Figure 1E). Indeed, simulation of the wild-type network results in scaling of the signaling gradient (S ≈ 0) (Figure 1H). The robustness of scaling to changes in parameter range was high. In fact, systematic perturbations of the parameters along a ten-dimensional cube around the reference network confirmed that 97.5% of parameter sets had −0.25 < S < 0.25 in a wide range of the field (Figure S1).

Our analysis suggests that Pent may function as the expander in an expansion-repression motif that scales the Dpp gradient. Pent is therefore predicted to be essential for scaling (Figures 1I–1K). Moreover, scaling requires the repression of *pent* by Dpp, predicting that scaling will be lost if *pent* is constitutively expressed (Figures 1L–1N). To examine these predictions, we set out to compare the scaling of the Dpp activation gradient in discs of different sizes during growth. We follow the Dpp activity gradient using an antibody for phosphorylated Mad (pMad), representing the initial signaling event triggered by Tkv upon binding to Dpp (Figure 1C) [27]. To reliably compare different discs, we analyzed the spatial distribution of pMad in the posterior compartment dorsal to the DV midline, as identified by the expression pattern of Patched and Wingless (Figure 2A).

Consistent with previous results in wild-type discs [11], the pMad gradient expanded in proportion to disc size. The discs we analyzed varied by 2-fold (Figure S2), and the pMad gradients in those discs were practically identical when plotted as a function of the relative positions in the disc; for example, all gradients decayed by 10-fold at the middle of the disc (x = L/2), and by 4-fold at x = L/3 (Figures 2B and 2C). This observation is reflected in the scaling measure for wild-type discs: S ≈ 0 in the medial part of the disc (0.1 < x/L < 0.5; Figure 2D; see also Figure S2 for other measures of scaling). Assessing scaling accurately in the lateral part of the disc is difficult, as a result of the low levels of pMad. We note that scaling was observed from the mid-third instar until the onset of wandering stage larvae, lasting approximately 36 hr. Scaling may be harder to observe in younger discs because of their small size, or it may be that the gradient does not scale in these early phases. Discs of the wandering stages were excluded from the analysis as the gradient becomes weaker and sharper, reflecting perhaps physiological changes caused by hormonal signaling [28].

Next, we examined scaling in discs homozygous for a null allele of *pent.* As described previously [26], those discs were smaller in size (reduced 1.5-fold compared to wild-type discs), and pMad distribution was narrower (Figure 2E). Still, these discs grew, and we observed an over 2-fold variation in size between discs, which enabled us to examine scaling. As predicted, the pMad gradient in these discs did not scale with disc size: the profiles overlapped when plotted in standard rather than relative coordinates, and the scaling measure was consistently S ≈ −1 (Figures 2F–2H; Figure S2).

The pMad gradient in the *pent* mutant discs decreased sharply and was therefore localized mostly to the source region. To control for possible spatial effects due to the short range of the gradient, we examined scaling also in a $tkv^{-/+}$ heterozygous background. In these discs, the Dpp gradient is wider, likely reflecting reduced Dpp degradation by endocytosis. Heterozygocity for *tkv* changed the range of pMad profile and slightly increased the size of the discs [26]. Nonetheless, scaling was maintained (Figures 2I–2L) in accordance with the expansion-repression model, where the ability to scale is robust to changes in parameters affecting gradient shape. Notably, introducing a homozygous *pent* null allele into the $tkv^{-/+}$ background abolished scaling (S ≈ −1), although the gradient range was now significantly wider and comparable to wild-type discs (Figures 2M–2P; Figure S2).

(C) Illustration of the interactions of Dpp, Thickveins (Tkv), Dally, and Pentagone (Pent). Dpp forms a complex with Tkv, where Dally acts as a coreceptor. Interaction of Dally with Pent may sequester Dally from interacting with Tkv. Interaction of Tkv and Dpp triggers a signaling cascade whose initial phase is the phosphorylation of Mad. Medial cells are closer to the source of Dpp; therefore, Dpp concentrations and pMad signaling are high, leading to only basal expression levels of *tkv* and *dally* and complete suppression of *pent* expression. In lateral cells, Dpp levels are low and signaling is weaker, which alleviates the repression of *tkv*, *dally*, and *pent*. Pent is secreted from lateral cells and spreads uniformly, thereby affecting the entire compartment.

(D) Interactions of Dpp, Tkv, Dally, and Pent used to model the Dpp morphogen gradient. Dpp forms a complex with Tkv. The complex attenuates the expression of *tkv* and *dally* and completely suppresses *pent* expression. Following complex formation, Dpp is degraded, whereas Tkv is recycled. Dally increases the affinity between Tkv and Dpp. Dally and Pent form a complex that reduces the effect of Dally on the Tkv-Dpp interaction, leading effectively to reduction in Dpp degradation rate and expansion of the gradient. It is not clear how the Dally-Pent complex modulates the gradient. Other possibilities such as increasing Dpp diffusion and full network schemes are shown in Figure S1.

(E) The scaling measure (S) quantifies scaling in a position-dependent manner. S = 0 when scaling is perfect (blue region, −0.25 < S < 0.25); S = −1 when the gradient is independent of the length of the field (red region, −1.25 < S < −0.75); S > 0 when the gradient profile expands relatively more than the length of the field.

(F–N) Numerical solutions of the model for wild-type (F–H), *pent* null (I–K), and constitutive ubiquitous *pent* expression in the entire field (L–N) for various sizes of the morphogenic field. Position in the disc is shown in standard coordinates (x) (F, I, and L) and relative coordinates (x/L) (G, J, and M). The y axis shows the normalized levels of the DppTkv complex in logarithmic scale. Length of the field is in micrometers. The legend in (F), (I), and (L) indicates the lengths in micrometers of each profile. The scaling measure is shown for each case in (H), (K), (N). Light shades of gray denote short fields, and dark shades denote longer fields. Wild-type profiles overlap in relative coordinates (G), whereas *pent* null profiles overlap in standard coordinates (I), and in ubiquitous *pent* long profiles are wider than short profiles also in relative coordinates (M). These observations are reflected in the scaling measure (H, K, N). See Experimental Procedures and Table S2 for model equations and parameters and Figure S1 for robustness analysis of the scaling measure.

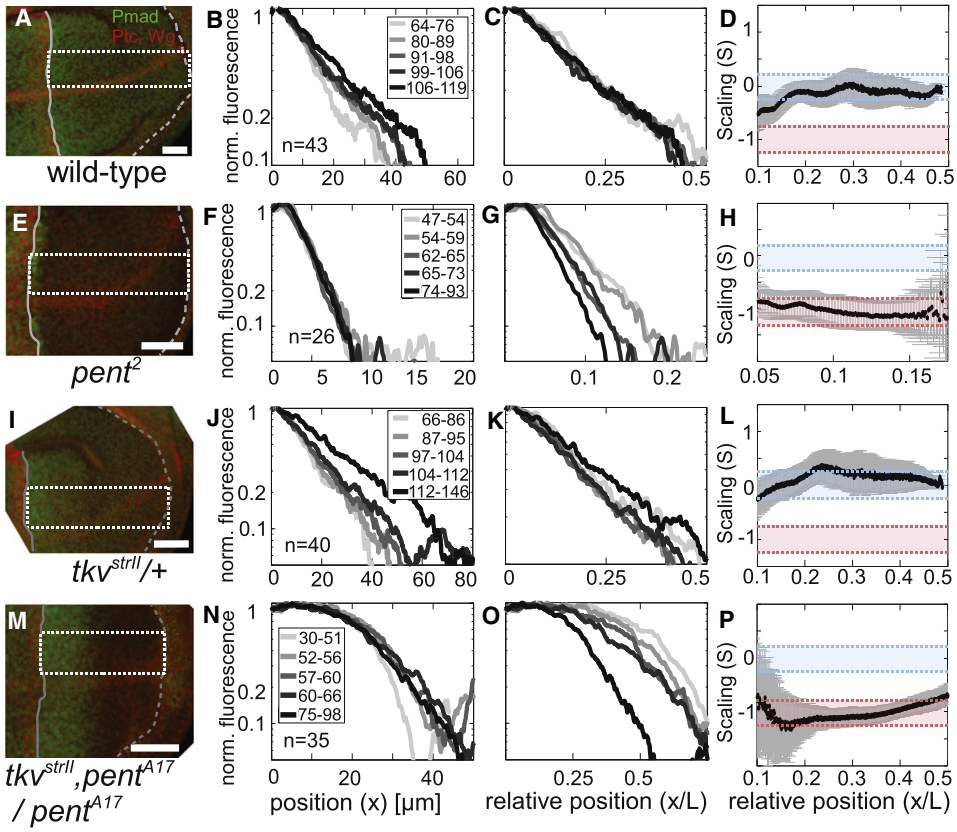

Figure 2. Scaling of pMad Is Dependent on Expression of *pent*

(A–D) Scaling of wild-type wing imaginal discs.

(A) The posterior compartment of a wild-type wing imaginal disc. pMad antibody staining is shown in green, Wg and Ptc in red; the white rectangle marks the area used for analysis of the profiles. The dashed gray line marks the edge of the wing pouch, and the solid gray line marks the AP boundary; scale bar represents 20 μm.

(B and C) Profiles of pMad gradients in wild-type discs of various sizes in standard (B) and relative (C) coordinates, y axis in log scale. Profiles were grouped by the length of the posterior compartment of the disc, and the range of lengths of each group in micrometers is given in the legend of (B). The total number of discs used for the analysis in (B)–(D) is indicated in (B); the size of each group is n = 5. Light shades of gray are used for small discs and darker shades for large discs.

(D) The scaling measure quantifies scaling of the gradients. Light blue marks the domain of perfect scaling, and light red marks the domain of no scaling.

(E–H) Loss of scaling in homozygous $pent^{2}$ wing imaginal discs, in which *pent* is not expressed. The gradient is extremely sharp, and the discs are smaller. Markings are shown as in (A)–(D).

(I–L) Scaling is maintained in tkv^{strII} heterozygous discs in which only one functional copy of *tkv* is expressed. The gradient is slightly wider than in wild-type discs, and the discs are larger. Markings are shown as in (A)–(D).

(M–P) Scaling is lost in $pent^{A17}$, $tkv^{strII}/pent^{A17}$discs, a background combining lack of *pent* expression with heterozygosity for *tkv*. The gradient is wider and more amenable for analysis. Markings are shown as in (A)–(D).

Error bars for S at each position were estimated by the standard deviation of S following bootstrapping the data (see Supplemental Information). See Figure S2 for distribution of lengths of the profiles used in the analysis.

A direct prediction of our expansion-repression model is that scaling requires the repression of *pent* expression by Dpp signaling. In fact, we not only predict that scaling will be lost when *pent* expression becomes constitutive but also expect a scaling overshoot, reflecting the high levels of Pentagone accumulation, which will cause the gradient to expand more than the growth of the disc. To examine this prediction, we expressed *pent* in the entire posterior compartment using the *engrailed (en)-Gal4* driver and measured the resulting pMad gradient. As expected, scaling was lost: the gradients do not overlap in the relative coordinates, and we observe the predicted overshoot, with gradients of large discs becoming wider than those of small discs (Figures 3A–3C). The scaling overshoot was also captured by the positive scaling measure obtained ($S > 0$; Figure 3D; Figure S3). Mild overexpression of *pent* by growing the larvae at 18°C resulted in significant yet reduced overscaling, with smaller positive values of *S* (Figures 3E–3I).

Taken together, our data identify an expansion-repression circuit motif that underlies the scaling of the Dpp activity gradient in the *Drosophila* wing imaginal disc. Pentagone, which functions as an expander in this system, scales the gradient in the entire disc. *pent* expression is restricted to the lateral cells as a result of repression by Dpp signaling [26]. Through its diffusible, nonautonomous effect on Dpp distribution, Pentagone couples the information on the position of the edge of the disc (i.e., size), to the overall distribution of the patterning gradient, thus executing scaling.

The expansion-repression motif provides scaling by effectively implementing an integral feedback controller over tissue

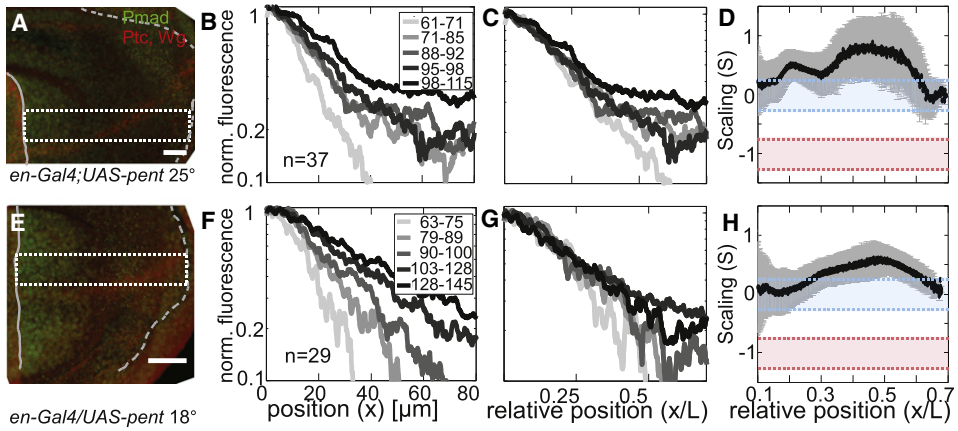

Figure 3. Constitutive Expression of *pent* in the Posterior Domain Leads to Overexpansion of the pMad Profile

(A–D) *pent* was constitutively expressed in the posterior compartment of the wing imaginal disc using the *en-Gal4* driver and *UAS-pent* at 25°C. The gradient expands more than the discs grow during development. Markings are shown as in Figure 2.

(E–H) Panels are the same as in (A)–(D). In this case, the larvae were grown at 18°C, leading to lower activation of the Gal4-UAS system. Consequently, overexpansion of the gradient is less pronounced. Markings are shown as in Figure 2.

See Figure S3 for distribution of lengths of the profiles used in the analysis.

size [1, 29]. We showed previously that this motif explains scaling of the Bmp gradient in the early *Xenopus laevis* embryo [30–33]. Here, we present an additional example, where this motif is implemented by a completely different molecular circuit, to scale the Dpp gradient in the *Drosophila* wing imaginal disc. The expansion-repression motif can be readily utilized by a variety of other molecular mechanisms, suggesting its general applicability in scaling morphogen gradients during development.

Experimental Procedures

Model Equations

$$\frac{\partial[Dpp]}{\partial t} = D_{Dpp}([Dally],[DallyPent])\nabla^2[Dpp] - k^{+}_{DppTkv}([Dally],[DallyPent])[Dpp][Tkv] + k^{-}_{DppTkv}[DppTkv] - \beta_{Dpp}[Dpp]$$

$$\frac{\partial[Pent]}{\partial t} = D_{Pent}\nabla^2[Pent] - k^{+}_{DallyPent}[Dally][Pent] + k^{-}_{DallyPent}[DallyPent] - \beta_{Pent}[Pent] + \alpha_{Pent}([DppTkv])$$

$$\frac{\partial[Tkv]}{\partial t} = -k^{+}_{DppTkv}([Dally],[DallyPent])[Dpp][Tkv] + k^{-}_{DppTkv}[DppTkv] + \beta_{DppTkv}[DppTkv] - \beta_{Tkv}[Tkv] + \alpha^{0}_{Tkv} + \alpha_{Tkv}([DppTkv])$$

$$\frac{\partial[Dally]}{\partial t} = -k^{+}_{DallyPent}[Dally][Pent] + k^{-}_{DallyPent}[DallyPent] - \beta_{Dally}[Dally] + \alpha^{0}_{Dally} + \alpha_{Dally}([DppTkv])$$

$$\frac{\partial[DppTkv]}{\partial t} = k^{+}_{DppTkv}([Dally],[DallyPent])[Dpp][Tkv] - k^{-}_{DppTkv}[DppTkv] - \beta_{DppTkv}[DppTkv]$$

$$\frac{\partial[DallyPent]}{\partial t} = k^{+}_{DallyPent}[Dal][Pent] - k^{-}_{DallyPent}[DallyPent]$$

[*P*] denotes the concentration of species *P*, and $k^{+(-)}_{PQ}$ denotes the association (dissociation) constant of *P* and *Q* (the complex *PQ*). D_P is the diffusion coefficient, β_P the degradation rate, and α^0_P the basal production rate of *P*. $\alpha_P([DppTkv])$ is the production rate of P, regulated by DppTkv complex, modeled as a Hill function for a repression threshold T_P and a Hill coefficient H_P. Dpp is produced with a flux η from x = 0. Dpp diffusion rate is increased by Dally and DallyPent levels, and the association rate between Dpp and Tkv is modulated by both Dally and DallyPent complex levels. See Tables S1 and S2 for values of parameters used in numerical solutions and explicit formulation of regulatory functions and for the equations for the model of the expansion-repression mechanism shown in Figure 1B.

Fly Strains

The following lines were used: y^1w^{1118} (wild-type), $pent^2$ and $pent^{A17}$ (*pent* null) [26], *UAS-pent/MKRSb* [26], and tkv^{strII}, *en-Gal4* from the Bloomington Stock Center.

Immunohistochemistry and Image Analysis

Third-instar larvae were dissected before wandering stage, fixed with 4% formaldehyde, and washed with 0.1 Triton X-100. Staining was carried out using rabbit anti-pSmad1/5/8 (1:250; obtained from E. Laufer); 4D4 mouse anti-Wg [32] (1:50) and Apa1 mouse anti-Ptc [33] (1:50) were obtained from the Hybridoma Bank. Images were obtained using a Zeiss LSM510 confocal microscope and analyzed in MATLAB. Profiles were grouped according to size such that five average sizes were used for the analysis, each group composed of profiles of similar sizes.

Scaling Measure

The scaling measure was calculated by the following, for each threshold $0.01 < T < 0.9$ within the normalized signaling level ($0.1 < T < 0.9$ for experimental data):

$$S = \frac{-1}{\zeta}\frac{2}{n(n-1)}\sum_{\{(i,j)|L_i>L_j\}}\frac{z_i - z_j}{0.5(z_i + z_j)}$$

n is the number of average profiles, L_i is the length of the i^{th} profile, and z_i is the relative position x_i/L_i where a threshold T was met in the i^{th} profile. ζ is the nonnormalized scaling measure in case there is no scaling: $\zeta = 2/n(n-1)\sum_{\{(i,j)|L_i>L_j\}} L_i - L_j/0.5(L_i + L_j)$. ζ is threshold independent and therefore position independent. We used a closely spaced set of thresholds to span the relevant region in the AP axis of the posterior compartment.

Supplemental Information

Supplemental Information includes eight equations, three figures, three tables, and Supplemental Experimental Procedures and can be found with this article online at doi:10.1016/j.cub.2011.07.015.

Acknowledgments

We thank E. Laufer for the pSmad1/5/8 antibody and the members of our groups for discussions and help with the experiments and analysis.

D.B.-Z. is supported by the Adams Fellowship Program of the Israeli Academy of Sciences and Humanities. This work was supported by the European Research Council, Israel Science Foundation, Minerva, and the Helen and Martin Kimmel Award for Innovative Investigations to N.B. B.-Z.S. holds the Hilda and Cecil Lewis Professorial Chair in Molecular Genetics.

Received: May 24, 2011
Revised: June 20, 2011
Accepted: July 12, 2011
Published online: August 11, 2011

References

1. Ben-Zvi, D., and Barkai, N. (2010). Scaling of morphogen gradients by an expansion-repression integral feedback control. Proc. Natl. Acad. Sci. USA *107*, 6924–6929.
2. Umulis, D.M. (2009). Analysis of dynamic morphogen scale invariance. J. R. Soc. Interface *6*, 1179–1191.
3. Gregor, T., Bialek, W., van Steveninck, R.R.R., Tank, D.W., and Wieschaus, E.F. (2005). Diffusion and scaling during early embryonic pattern formation. Proc. Natl. Acad. Sci. USA *102*, 18403–18407.
4. O'Connor, M.B., Umulis, D., Othmer, H.G., and Blair, S.S. (2006). Shaping BMP morphogen gradients in the Drosophila embryo and pupal wing. Development *133*, 183–193.
5. McHale, P., Rappel, W.J., and Levine, H. (2006). Embryonic pattern scaling achieved by oppositely directed morphogen gradients. Phys. Biol. *3*, 107–120.
6. Gregor, T., McGregor, A.P., and Wieschaus, E.F. (2008). Shape and function of the Bicoid morphogen gradient in dipteran species with different sized embryos. Dev. Biol. *316*, 350–358.
7. Howard, M., and ten Wolde, P.R. (2005). Finding the center reliably: Robust patterns of developmental gene expression. Phys. Rev. Lett. *95*, 208103.
8. Aegerter-Wilmsen, T., Aegerter, C.M., and Bisseling, T. (2005). Model for the robust establishment of precise proportions in the early Drosophila embryo. J. Theor. Biol. *234*, 13–19.
9. Lander, A.D., Nie, Q., Vargas, B., and Wan, F.Y.M. (2011). Size-normalized robustness of Dpp gradient in Drosophila wing imaginal disc. J. Mech. Mater. Struct. *6*, 321–350.
10. Teleman, A.A., and Cohen, S.M. (2000). Dpp gradient formation in the Drosophila wing imaginal disc. Cell *103*, 971–980.
11. Wartlick, O., Mumcu, P., Kicheva, A., Bittig, T., Seum, C., Julicher, F., and Gonzalez-Gaitan, M. (2011). Dynamics of Dpp Signaling and Proliferation Control. Science *331*, 1154–1159.
12. Hufnagel, L., Teleman, A.A., Rouault, H., Cohen, S.M., and Shraiman, B.I. (2007). On the mechanism of wing size determination in fly development. Proc. Natl. Acad. Sci. USA *104*, 3835–3840.
13. Affolter, M., and Basler, K. (2007). The Decapentaplegic morphogen gradient: From pattern formation to growth regulation. Nat. Rev. Genet. *8*, 663–674.
14. Schwank, G., and Basler, K. (2010). Regulation of Organ Growth by Morphogen Gradients. Cold Spring Harb. Perspect. Biol. *2*, 16.
15. Strigini, M., and Cohen, S.M. (2000). Wingless gradient formation in the Drosophila wing. Curr. Biol. *10*, 293–300.
16. Rogulja, D., Rauskolb, C., and Irvine, K.D. (2008). Morphogen control of wing growth through the fat signaling pathway. Dev. Cell *15*, 309–321.
17. Umulis, D., O'Connor, M.B., and Blair, S.S. (2009). The extracellular regulation of bone morphogenetic protein signaling. Development *136*, 3715–3728.
18. Entchev, E.V., Schwabedissen, A., and Gonzalez-Gaitan, M. (2000). Gradient formation of the TGF-beta homolog Dpp. Cell *103*, 981–991.
19. Lecuit, T., and Cohen, S.M. (1998). Dpp receptor levels contribute to shaping the Dpp morphogen gradient in the Drosophila wing imaginal disc. Development *125*, 4901–4907.
20. Crickmore, M.A., and Mann, R.S. (2006). Hox control of organ size by regulation of morphogen production and mobility. Science *313*, 63–68.
21. Akiyama, T., Kamimura, K., Firkus, C., Takeo, S., Shimmi, O., and Nakato, H. (2008). Dally regulates Dpp morphogen gradient formation by stabilizing Dpp on the cell surface. Dev. Biol. *313*, 408–419.
22. Hufnagel, L., Kreuger, J., Cohen, S.M., and Shraiman, B.I. (2006). On the role of glypicans in the process of morphogen gradient formation. Dev. Biol. *300*, 512–522.
23. Fujise, M., Takeo, S., Kamimura, K., Matsuo, T., Aigaki, T., Izumi, S., and Nakato, H. (2003). Daily regulates Dpp morphogen gradient formation in the Drosophila wing. Development *130*, 1515–1522.
24. Yan, D., and Lin, X.H. (2009). Shaping Morphogen Gradients by Proteoglycans. Cold Spring Harb. Perspect. Biol. *1*, 16.
25. Crickmore, M.A., and Mann, R.S. (2007). Hox control of morphogen mobility and organ development through regulation of glypican expression. Development *134*, 327–334.
26. Vuilleumier, R., Springhorn, A., Patterson, L., Koidl, S., Hammerschmidt, M., Affolter, M., and Pyrowolakis, G. (2010). Control of Dpp morphogen signalling by a secreted feedback regulator. Nat. Cell Biol. *12*, 611–617.
27. Heldin, C.H., Miyazono, K., and tenDijke, P. (1997). TGF-beta signalling from cell membrane to nucleus through SMAD proteins. Nature *390*, 465–471.
28. Truman, J.W., and Riddiford, L.M. (2007). The morphostatic actions of juvenile hormone. Insect Biochem. Mol. Biol. *37*, 761–770.
29. Lander, A.D. (2011). Pattern, Growth, and Control. Cell *144*, 955–969.
30. Ben-Zvi, D., Shilo, B.Z., Fainsod, A., and Barkai, N. (2008). Scaling of the BMP activation gradient in Xenopus embryos. Nature *453*, 1205–1211.
31. Barkai, N., and Ben-Zvi, D. (2009). 'Big frog, small frog'- maintaining proportions in embryonic development. FEBS J. *276*, 1196–1207.
32. Brook, W.J., and Cohen, S.M. (1996). Antagonistic interactions between Wingless and decapentaplegic responsible for dorsal-ventral pattern in the Drosophila leg. Science *273*, 1373–1377.
33. Capdevila, J., Estrada, M.P., Sanchezherrero, E., and Guerrero, I. (1994). The Drosophila Segment Polarity Gene patched Interacts with Decapentaplegic in Wing Development. EMBO J. *13*, 71–82.